Inorganic Chemistry

Article

pubs.acs.org/IC

Solid-State NMR Structure Characterization of a ^{13}CO-Labeled Ir(I) Complex with a *P,N*-Donor Ligand Including Ultrafast MAS Methods

Andrey A. Tregubov,[‡,∥] Rasmus Linser,[†,∥] Khuong Q. Vuong,[‡] Aditiya Rawal,[†] John D. Gehman,[§] and Barbara A. Messerle*[,‡]

[‡]School of Chemistry, University of New South Wales, Sydney, 2052, New South Wales, Australia

[†]Mark Wainwright Analytical Centre, Nuclear Magnetic Resonance Facility, University of New South Wales, Sydney, 2052, New South Wales, Australia

[§]Bio21 Institute, University of Melbourne, Melbourne, 3010, Victoria, Australia

Supporting Information

ABSTRACT: The structural characterization of a ^{13}CO-labeled Ir(I) complex bearing an *P,N*-donor ligand (1-[2-(diphenylphosphino)ethyl]pyrazole), [Ir(PyP)(^{13}CO)Cl] is demonstrated using a series of tailored solid-state NMR techniques based on ultrafast (60 kHz) Magic Angle Spinning (MAS), which facilitates correlations with narrow proton linewidths. Our 1D ^{1}H MAS and 2D ^{13}C and ^{31}P CP-MAS NMR spectra provided structural information similar to that obtained using NMR spectroscopy in solution. We employed high-resolution 2D solid-state correlation spectroscopy (^{1}H−^{13}C HETCOR, ^{1}H−^{31}P correlation) to characterize the networks of dipolar couplings between protons and carbon/phosphorus. ^{1}H−^{1}H SQ−SQ correlation spectra showed the dipolar contacts between all protons in a similar fashion to its solution counterpart, NOESY. The use of the ^{1}H single quantum/double quantum experiments made it possible to observe the dipolar-coupling contacts between immediately adjacent protons. Additionally, internuclear ^{13}CO−^{31}P distance measurements were performed using REDOR. The combination of all of these techniques made it possible to obtain comprehensive structural information on the molecule [Ir(PyP)(^{13}CO)Cl] in the solid state, which is in excellent agreement with the single crystal X-ray structure of the complex, and demonstrates the enormous value of ultrafast MAS NMR techniques for a broad range of future applications.

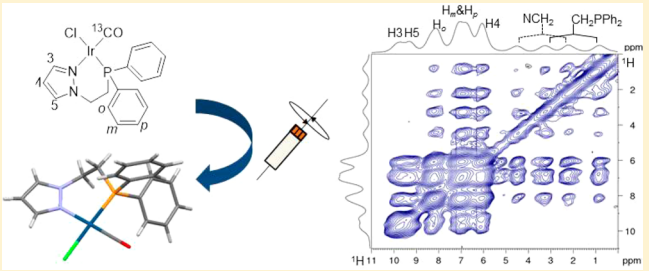

INTRODUCTION

Nowadays, transition-metal organometallic complexes are widely used as catalysts in organic and polymer chemistry.[1] Homogeneous catalysis using organometallic complexes has achieved tremendous success in understanding the mechanisms of catalyzed reactions. However, the broad industrial application of these systems is limited due to problems related to recycling and reuse of the catalysts. The immobilization of these complexes on insoluble supports aims to combine the advantages of both homo- and heterogeneous catalysis (straightforward characterization and ease of separation and reuse, respectively).[2] Homogeneous organometallic complexes can be readily characterized using conventional methods such as single crystal X-ray diffraction and NMR in solution. However, these methods cannot be applied to supported complexes due to the insoluble and disordered nature of the supported complexes. In this case, solid-state NMR spectroscopy has the possibility of providing information about the structure of systems which cannot be characterized using diffraction methods[3−5] and can also be applicable for *in situ* experiments.[6,7]

A feature of solid-state NMR spectroscopy that distinguishes it from its solution counterpart is the presence of distance and orientation dependent (*i.e.*, anisotropic) interactions which are averaged to zero in solution. Indeed, these interactions can provide important information about the structure of catalytically active molecules immobilized on the surface of a solid support which are not readily characterized using diffraction methods.[8−11] Numerous studies of inorganic materials or organometallic catalysts have used solid-state NMR to obtain structural information. Examples of such studies have involved alumina-supported,[12,13] silica-supported,[8,14,15] or Zr-bound catalysts,[16,17] and many more.

For inorganic solids, the development of technologies which utilize ultrafast MAS is a great step forward. Ultrafast MAS significantly reduces spinning sidebands arising from chemical shift anisotropy and effectively averages the effect of the strong homonuclear dipolar coupling between high γ nuclei such as ^{1}H and ^{19}F. More importantly, however, the drastically improved resolution in the proton/fluorine dimension is extremely useful

Received: January 19, 2014
Published: July 3, 2014

dx.doi.org/10.1021/ic500128y | *Inorg. Chem.* 2014, 53, 7146−7153

for a wide range of correlation experiments. Therefore, ultrafast MAS significantly has now expanded the existing possibilities for characterization of natural-abundance materials.[18,19] Previous work devoted to the characterization of metal complexes using ^{1}H and ^{13}C solid-state NMR has been mainly focused on paramagnetic systems.[20,21] For example, Dittmer et al. used a series of solid-state NMR techniques employed under 30 kHz MAS to study the structure of a paramagnetic Cu−cyclam complex in the solid state.[22] With intermediate MAS rates, large differences in resonance frequencies can compensate for the effect of strong $^{1}H-^{1}H$ dipolar coupling, leading to well-resolved resonances in the proton dimension. However, this methodology cannot easily be applied to diamagnetic complexes with a narrow range in their ^{1}H NMR spectra (of up to 15 ppm). Here, we present the structural characterization of the diamagnetic ^{13}CO-labeled Ir(I) complex with the *P,N*-donor ligand (1-[2-(diphenylphosphino)ethyl]-pyrazole)), [Ir(PyP)(^{13}CO)Cl] (Figure 1), using a series of solid-state NMR

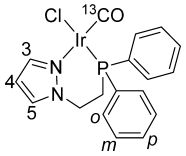

Figure 1. [Ir(PyP)(^{13}CO)Cl].

techniques (MAS, CP-MAS, $^{1}H-^{13}C$ HETCOR, $^{1}H-^{31}P$ correlation, $^{1}H-^{1}H$ SQ-SQ correlation, ^{1}H SQ-DQ correlation, and REDOR). A number of these experiments employed ultrafast (60 kHz) MAS yielding excellent proton chemical shift resolution. The results obtained are compared with those from the crystal structure of the previously reported unlabeled analogue [Ir(PyP)(CO)Cl] and can be considered as good groundwork for characterization of the related Rh(I) complexes with bidentate *N,N*- and *P,N*-donor ligands immobilized on the carbon surface via robust C−C bonds.[23]

EXPERIMENTAL SECTION

Synthesis of [Ir(PyP)(^{13}CO)Cl]. The complex [Ir(PyP)(^{13}CO)Cl] was synthesized using the same procedure as that used for the synthesis of the unlabeled analogue [Ir(PyP)(CO)Cl][24] with the exception that ^{13}C-enriched carbon monoxide was used instead of carbon monoxide.

^{1}H NMR (300 MHz, CD_2Cl_2): δ 8.49 (d, ^{3}J(H4−H3) = 2.3 Hz, 1H, **H**3), 7.84−7.77 (m, 4H, *o*-C**H** of PPh_2), 7.55 (d, 1H, ^{3}J(H4−H5) = 2.3 Hz, **H**5), 7.49−7.45 (m, 6H, *m*-C**H** and *p*-C**H** of PPh_2), 6.36 (apparent t, 1H, ^{3}J(H3−H4, H5−H4) = 2.3 Hz, **H**4), 4.58 (m, 2H, N**C**H_2), 2.73 (m, 2H, **C**$H_2$$PPh_2$) ppm.

$^{31}P\{^{1}H\}$ NMR (121 MHz, CD_2Cl_2): δ 10.5 (d, ^{2}J(^{13}CO-P) = 13.8 Hz) ppm.

$^{13}C\{^{1}H\}$ NMR (75 MHz, CD_2Cl_2): δ 174.3 (enhanced signal, d, ^{2}J(P−^{13}CO) = 13.8 Hz, ^{13}**C**O), 144.0 (**C**3), 133.6 (**C**5), 133.2 (d, ^{1}J(P−C) = 61.8 Hz, *ipso*-**C** of PPh_2), 132.9 (d, ^{2}J(P−C) = 10.9 Hz, *o*-**C** of PPh_2), 130.8 (d, ^{4}J(P−C) = 2.5 Hz, *p*-**C** of PPh_2), 128.5 (d, ^{3}J(P−C) = 10.9 Hz, *m*-**C** of PPh_2), 105.9 (**C**4), 49.0 (d, ^{2}J(P−C) = 2.2 Hz, N**C**H_2), 27.1 (d, ^{1}J(P−C) = 34.9, **C**$H_2$$PPh_2$) ppm.

The NMR experimental details are presented in the Supporting Information.

RESULTS

1D Solid-State NMR Spectra of [Ir(PyP)(^{13}CO)Cl]. ^{1}H MAS spectra of [Ir(PyP)(^{13}CO)Cl] acquired at a MAS rate of 60 kHz are shown in Figure 2a. This spectrum contains well-resolved resonances both for aliphatic (0−5 ppm) and aromatic (5−10 ppm) protons. The $^{1}H\{^{31}P\}$ NMR spectrum of [Ir(PyP)(^{13}CO)Cl] recorded in CD_2Cl_2 (see the Supporting Info) has two triplets in the aliphatic region due to the two pairs of methylene protons NCH_2 and CH_2PPh_2, where the two geminal protons of a methylene group are magnetically equivalent. On the other hand, the solid-state spectrum shown in Figure 2b contains four peaks in the aliphatic region, which can be attributed to the four protons of the two CH_2 groups in the molecule. The presence of four peaks in the 0−5 ppm region indicates the nonequivalence of the geminal methylene protons (NCH_2 and CH_2PPh_2) in the solid state. The resonances in the aromatic region of the spectrum shown in Figure 2a can be attributed to the protons of the pyrazole ring and phenyl groups. The detailed assignment of these peaks was performed after acquisition of 2D correlation spectra (see below).

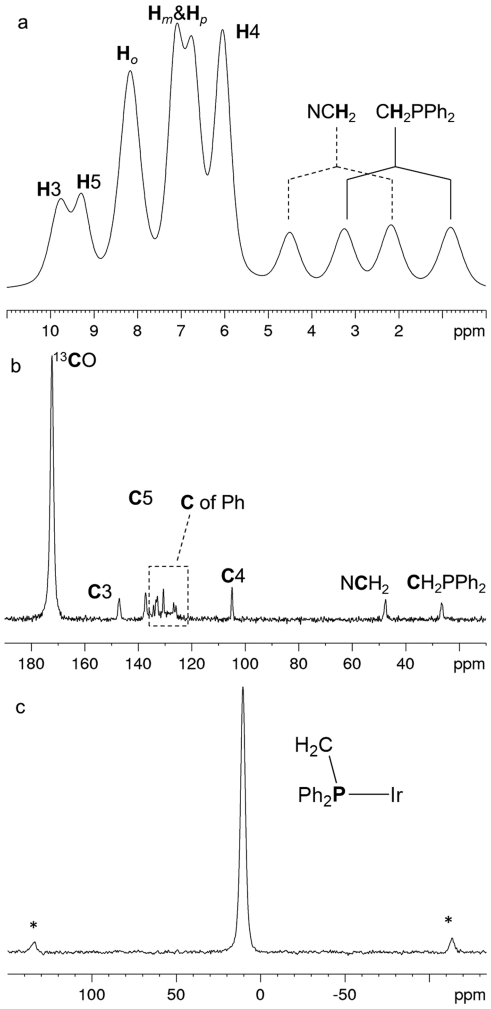

Figure 2. 1D NMR spectra of [Ir(PyP)(^{13}CO)Cl]: (a) ^{1}H MAS (ν_r = 60 kHz, $\omega_0/2\pi$ = 700 MHz), (b) ^{13}C CP-MAS (ν_r = 15 kHz, $\omega_0/2\pi$ = 300 MHz), (c) ^{31}P CP-MAS (ν_r = 15 kHz, $\omega_0/2\pi$ = 300 MHz; * denotes spinning sidebands).

The ^{13}C CP-MAS NMR spectrum of [Ir(PyP)(^{13}CO)Cl] is shown in Figure 2b. This spectrum is quite similar to that of the same compound recorded in solution. The enhanced resonance at 172.3 ppm is due to the ^{13}C-isotope-enriched carbonyl carbon. The resonances at 147.1, 137.2, and 104.8 ppm are due to C3, C5, and C4 carbons of the pyrazole ring, respectively. A

dx.doi.org/10.1021/ic500128y | Inorg. Chem. 2014, 53, 7146−7153

number of resonances at 135−125 ppm can be attributed to the carbons of the phenyl groups. Finally, the resonances at 47.2 and 26.4 ppm can be assigned to the methylene carbons of the NCH_2 and CH_2PPh_2 groups, respectively.

The ^{31}P CP-MAS NMR spectrum of [Ir(PyP)(^{13}CO)Cl] shown in Figure 2c contains one main peak at 10.4 ppm, assigned to the phosphine group bound to the Ir metal center.

In summary, ^{1}H MAS and ^{13}C and ^{31}P CP MAS spectra provide information similar to that available from the solution NMR. However, some important distance/orientation-dependent information (see in the following) is lost due to this averaging to zero under MAS.

2D Correlation Spectroscopy. *$^{1}H-^{13}C$ HETCOR.* The assignment of resonances due to aliphatic and aromatic protons in the ^{1}H MAS spectrum (Figure 2a) was accomplished by means of a $^{1}H-^{13}C$ heteronuclear SQ−SQ experiment (Figure 3). This spectrum comprises all correlations between protons

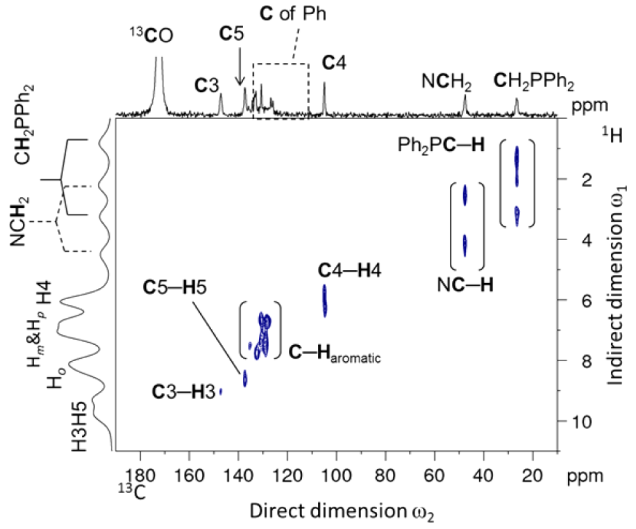

Figure 3. $^{1}H-^{13}C$ HETCOR spectrum of [Ir(PyP)(^{13}CO)Cl] acquired at an MAS rate of 12 kHz, using a CP contact time of 150 μs.

and carbons that are close in space. All resonances due to pyrazolyl carbons at 147.1, 137.2, and 104.8 ppm (C3, C5, and C4 carbons of the pyrazole ring, respectively) in the direct dimension (ω_2) correlate with the respective resonances at 9.75, 9.29, and 6.05 ppm due to pyrazole protons (H3, H5, and H4 protons of the pyrazole ring, respectively) in the indirect dimension (ω_1).

The resonance at 47.2 ppm due to NCH_2 carbons in the direct dimension (ω_2) correlates with two proton resonances at 4.5 and 2.2 ppm in the indirect dimension (ω_1). Similar correlations can be seen for the CH_2PPh_2 group: the resonance at 26.4 ppm due to the CH_2PPh_2 carbons in the direct dimension (ω_2) correlates with two resonances at 3.2 and 0.8 ppm in the indirect dimension (ω_1). The presence of two cross-peaks for each of the NCH_2 and CH_2PPh_2 groups indicates the nonequivalence of two geminal methylene protons in these groups in the solid state. Each pair, C_o-H_o, C_m-H_m, and C_p-H_p, also has two correlation peaks, due to the nonequivalence of the two phenyl groups of PPh_2 in the solid state. The enhanced resonance at 172.3 ppm due to ^{13}C enriched CO in the direct dimension does not correlate with any resonance in the indirect dimension, because the CO group does not have any protons in close proximity, which would be necessary for cross-polarization with the short contact time of 150 μs. Potentially, dynamic behavior of CO ligand could further affect a decrease of CP buildup efficiency at this site.

$^{1}H-^{31}P$ Correlation Experiments. The $^{1}H-^{31}P$ correlation spectrum acquired using a contact time of 4 ms is shown in Figure 4. This long spin-lock duration can be supplemented

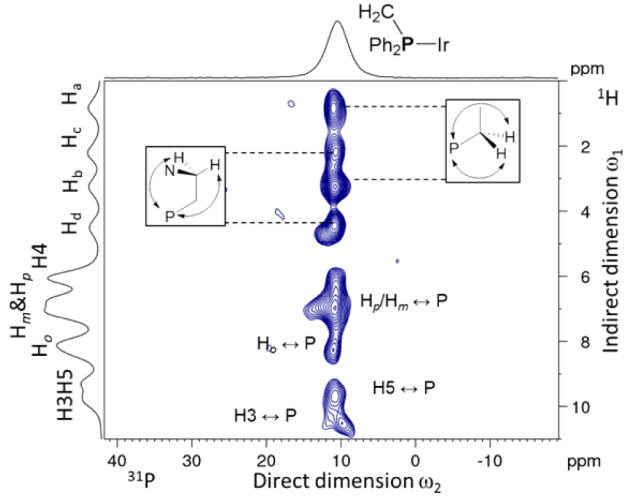

Figure 4. $^{1}H-^{31}P$ correlation spectrum of [Ir(PyP)(^{13}CO)Cl] acquired at a MAS rate of 60 kHz and a contact time of 4 ms.

with an additional PDSD (proton driven spin diffusion)[25,26] $^{1}H-^{1}H$ mixing time of different lengths (see Supporting Information) to provide long-range magnetization transfer to the phosphorus nucleus, which does not bear any directly bound protons. The spectrum contains four cross-peaks between resonances due to the aliphatic protons and the resonance due to the ^{31}P nucleus. The cross-peaks between resonances at 0.84 and 3.25 ppm in the indirect dimension (ω_1) and 10.4 ppm in the direct dimension (ω_2) have the highest intensity and therefore can be assigned to correlations between phosphorus and aliphatic protons of the CH_2PPh_2 group. The cross-peaks between the resonances due to the protons at 2.21 and 4.50 ppm in the indirect dimension (ω_1) and the resonance due to phosphorus at 10.4 ppm in the direct dimension (ω_2) were assigned to the correlation between aliphatic protons of the NCH_2 group and phosphorus. The intensities of the cross-peaks assigned to the correlations between the resonances due to more distant NCH_2 protons are lower than those assigned to the correlations between resonances due to CH_2PPh_2 protons and phosphorus.

The intense cross-peak between the resonance at 6.95 ppm in the indirect dimension (ω_1) and 10.4 ppm in the direct dimension (ω_2) was assigned to the correlation between the *para-* and *meta-* protons of the phenyl groups and phosphorus. The small cross-peak between the resonance at 8.17 ppm in the indirect dimension (ω_1) and at 10.4 ppm in the direct dimension (ω_2) was assigned to the correlation between *ortho-* protons of the phenyl groups and phosphorus. Another small cross-peak between the resonances at 9.29 ppm in the indirect dimension and 10.4 ppm in the direct dimension was assigned to the correlation between the H5 proton of the pyrazole ring and phosphorus. The neighboring cross-peak between the resonance at 9.75 ppm in the indirect dimension and the resonance at 10.4 ppm in the direct dimension has the weakest intensity in the spectrum and can be assigned to the correlation

dx.doi.org/10.1021/ic500128y | Inorg. Chem. 2014, 53, 7146−7153

between the H3 proton of the pyrazole ring and phosphorus. The correlation between the H4 proton of pyrazole and phosphorus is not seen in the spectrum shown in Figure 4 despite the excessive mixing of magnetization, because the distance between H4 and the PPh_2 is too large to establish a dipolar coupling sufficiently large for effective magnetization transfer (6.15 Å) at 60 kHz spinning rates. On acquisition of the same $^1H-^{31}P$ correlation experiment with a contact time of 1 ms (see Supporting Information), the intensity of signal transfer decreased; however, no additional information on internuclear distances could be established.

The $^1H-^{31}P$ correlation experiment here is useful for observing the heteronuclear dipolar-coupling contacts between ^{31}P and ^1H. Even though the intensities of cross-peaks which represent these contacts can be considered as a rough, qualitative indication of relative $^1H-^{31}P$ internuclear distances, the magnetization transfers are heavily influenced by spin diffusion processes among the numerous protons in the aliphatic ligand. In order to obtain more precise distances of individual internuclear vectors, buildup rates of dipolar couplings, *e.g.* using TEDOR,[27] would preferentially have been applied and dilute protonation in an otherwise deuterated background could be used.[28] The same information can potentially be obtained from indirect detection (^1H) using a solid-state HSQC experiment,[29] which is useful when only small amounts of material (*e.g.*,^{13}C-labeled material) are available.

$^1H-^1H$ Through-Space SQ-SQ Correlation Experiment. The 2D $^1H-^1H$ SQ–SQ correlation spectrum of [Ir(PyP)-(^{13}CO)Cl] acquired at t_{mix} = 20 ms is shown in Figure 5a. This spectrum is fully symmetric as is the solution-state counterpart NOESY. It contains correlations between all dipolar-coupled pairs of protons of [Ir(PyP)(^{13}CO)Cl]. Figure 5b represents an expansion of the aliphatic region of the spectrum shown in Figure 5a. The two cross-peaks due to the correlations between H_b and H_d (at 3.25 ppm (ω_2) and 4.50 ppm (ω_1), respectively) and H_b and H_c (at 3.25 ppm (ω_2) and 2.21 ppm (ω_1), respectively) have the same intensity. The intensities of two cross-peaks due to the correlations between H_c and H_b (at 2.21 ppm (ω_2) and 3.25 ppm (ω_1), respectively) and H_c and H_a (at 2.21 ppm (ω_2) and 0.83 ppm (ω_1), respectively) are also the same. The fact that the intensities of these cross-peaks are the same pairwise indicates that these cross-peaks arise from pairs of protons that are most probably separated by the same distances. This shows that the distances between the proton H_b and protons H_d and H_c and between the proton H_c and protons H_b and H_a are the same. This is possible only if the methylene protons in the ethylene bridge between the pyrazole ring and the phosphine group are in an *anti*-conformation. The *anti*-conformation would also result in different distances between the proton H_a and protons H_c and H_d, and also in different distances between the proton H_d and the protons H_a and H_b. Indeed, the cross-peak between the resonance at 4.50 ppm (due to the H_d proton) in the indirect dimension and the resonance at 3.25 ppm (due to the proton H_b) in the direct dimension is significantly more intense than that between the resonance at 4.50 ppm due to the H_d protons and the resonance at 0.83 ppm due to H_a proton in the direct dimension. These results are in good agreement with the three-dimensional structure established using single crystal X-ray diffraction data for the unlabeled analogue [Ir(PyP)(CO)Cl] (Figure 6).[24] The assessment of atomic distances in this manner is purely qualitative. For a more quantitative assessment of internuclear

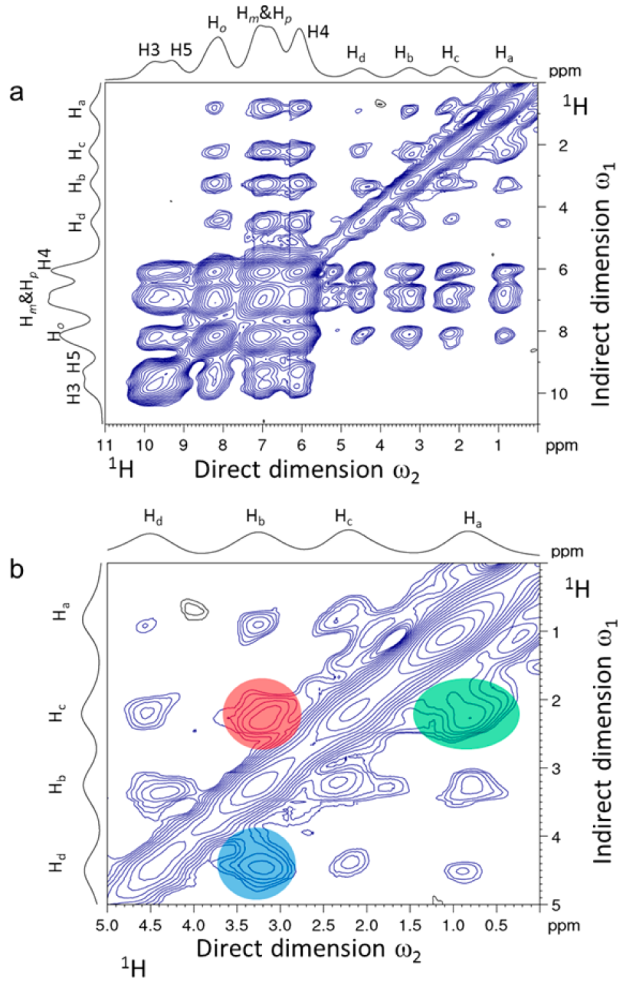

Figure 5. (a) A $^1H-^1H$ (700 MHz) SQ–SQ correlation spectrum of [Ir(PyP)(^{13}CO)Cl] in the solid state acquired at a MAS rate of 60 kHz, t_{mix} = 20 ms, 298 K. (b) An expansion of the aliphatic region of the spectrum (negative contours are shown in gray).

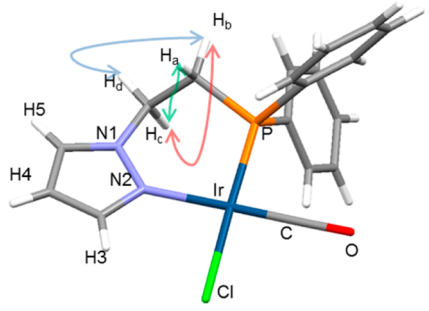

Figure 6. X-ray crystal structure of [Ir(PyP)(CO)Cl],[32] the unlabeled analogue of [Ir(PyP)(^{13}CO)Cl] (the arrow colors represent correlations between aliphatic protons highlighted in Figure 5b).

distances, buildup rates can potentially be extracted from a series of these 2D experiments (see Supporting Information for a series using PDSD mixing times of 2, 6, 20, 80, and 300 ms.) In analogy to the $^1H-^{31}P$ correlation, however, all peak intensities obtained for the dense proton network will necessarily be significantly influenced by spin diffusion among protons. In order to expand a qualitative description toward a quantitative assessment, proton dilution by deuterons[30] should be considered.

dx.doi.org/10.1021/ic500128y | Inorg. Chem. 2014, 53, 7146–7153

^{1}H SQ–DQ Correlation Experiment. The reintroduction of ^{1}H–^{1}H homonuclear dipolar coupling using the back-to-back (BABA)[31] sequence makes possible the observation of dipolar coupling contacts between immediately adjacent protons ($r_{H-H} \leq 4$ Å). The ^{1}H SQ–DQ correlation spectrum of [Ir(PyP)-(^{13}CO)Cl] shown in Figure 7 contains 10 pairs of off-diagonal peaks and one in-diagonal peak. The off-diagonal peaks represent the dipolar coupling interaction between unlike protons in close proximity, while the in-diagonal peak indicates the interaction between the same protons. As indicated by the X-ray structure available for the unlabeled analogue, these peaks can be divided into groups. The pairs of peaks indicated by red arrows represent dipolar coupling contacts within the molecule, while those pairs indicated by blue arrows represent intermolecular dipolar contacts. The intermolecular effect is due to crystal packing and is not to be expected for supported materials.

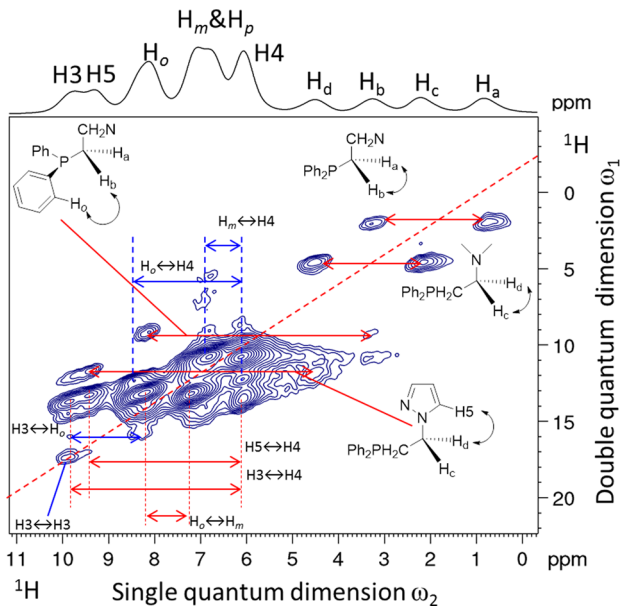

Figure 7. A ^{1}H (700 MHz) SQ–DQ correlation spectrum of [Ir(PyP)(^{13}CO)Cl] at a MAS rate of 60 kHz and 298 K with DQ evolution/reconversion over four rotor periods (red arrows represent contacts within the molecule; blue arrows indicate intermolecular contacts).

The dipolar coupling contacts within the molecule are represented by six pairs of off-diagonal peaks. The dipolar coupling interaction between geminal protons of the methylene groups NCH_2 and CH_2PPh_2 is represented by the presence of two pairs of off-diagonal peaks in the aliphatic region of the single-quantum dimension (ω_2). The two off-diagonal peaks at 3.25 and 0.83 ppm in ω_1 represent the dipolar-coupling interaction between geminal protons of the CH_2PPh_2 group, while the other two off-diagonal peaks at 4.50 and 3.21 ppm in ω_2 are due to the interaction between geminal protons in the NCH_2 group. The methylene H_b and H_d protons also interact with the *ortho*-protons of one phenyl group and the H5 proton of the pyrazole ring, respectively. The two off-diagonal peaks at 8.11 and 3.25 ppm in ω_2 arise from the dipolar coupling between one *ortho*-proton of a phenyl group and the proton H_b of CH_2PPh_2 group, while the two off-diagonal peaks at 9.29 and 4.50 ppm in ω_2 show the interaction between the proton H_d of the NCH_2 group and the H5 proton of the pyrazole ring. The pair of off-diagonal peaks at 8.11 and 6.96 ppm in ω_2 is due to the dipolar coupling between the *ortho*- and *meta*-protons of the phenyl groups. Finally, the dipolar coupling between H3/H5 and H4 protons of the pyrazole ring is confirmed by the presence of two sets of correlations. The off-diagonal peaks at 9.75 and 6.05 ppm in ω_2 are due to the dipolar coupling between the H3 and H4 protons of the pyrazole ring, while the off-diagonal peaks at 9.29 and 6.05 ppm in ω_2 are due to dipolar coupling between the H5 and H4 protons of the pyrazole ring.

The intermolecular dipolar coupling contacts are represented by the presence of three off-diagonal peaks and one in-diagonal peak in the spectrum shown in Figure 7. The off-diagonal peaks at 6.91 and 6.07 ppm in ω_2 show the dipolar coupling between the *meta*- protons of phenyl group and H4 protons of pyrazole ring belonging to two different molecules located within the same unit cell. The presence of off-diagonal peaks at 8.37 and 6.07 ppm in ω_2 can be explained by the dipolar coupling between an *ortho*- proton of a phenyl group and H4 protons. The couple of off diagonal peaks at 9.85 and 8.30 ppm in ω_2 indicates the coupling between *ortho*- protons of a phenyl group and H3 protons. Finally, the in-diagonal peak at 9.83 ppm in ω_2 is due to dipolar coupling between H3 protons belonging to neighboring molecules within the unit cell. This peak is slightly asymmetrical because of the overlay with two small off-diagonal peaks due to dipolar interaction between H3 and H5 protons within the molecule. The appearance of off- and in-diagonal peaks due to intermolecular dipolar coupling in the spectrum shown in Figure 7 can be explained by the data from the X-ray crystal structure for the unlabeled analogue [Ir(PyP)(CO)Cl]. The distances between protons participating in intermolecular dipolar coupling interaction are less than 4 Å. For example, the intermolecular contact H3↔H3 is 3.49 Å, which is enough to establish dipolar coupling contact under the recoupling sequence.

In summary, ^{1}H SQ–DQ correlation spectroscopy is a very useful tool for establishing dipolar coupling contacts between immediately adjacent protons in the solid state. This type of dipolar contact will be very important in the reconstruction of the three-dimensional structure of the molecule when no X-ray crystal structure is available. The intensities of off-diagonal peaks can be considered as a qualitative measure of distances between protons located within 4 Å to each other. The presence of off-diagonal and in-diagonal peaks due to protons engaged in the intermolecular dipolar coupling can potentially be prevented by dilution of the sample.

^{13}C–^{31}P Distance Measurements. The measurement of the ^{13}C–^{31}P internuclear distance in the [Ir(PyP)(^{13}CO)Cl] complex was performed using both ^{13}C{^{31}P} and ^{31}P{^{13}C} Rotational Echo Double Resonance (REDOR) experiments.[32] REDOR is a magic angle spinning experiment which provides high-precision measurement of selected internuclear distances. For each data point, two spectra are collected: The "full" reference spectrum (*e.g.*, that plotted in black in Figure 8) measures the regular signal decay during a given evolution time, just as one might routinely measure T_2 relaxation. The "dephased" spectrum (plotted in red in Figure 8) repeats the pulse sequence, but includes a number (N) of extra rotor-synchronized π-pulses, one per rotor period (T_r), which reintroduces the dipolar coupling. The effect is to accelerate apparent signal decay. The sum of the spectral intensity across the manifold of spinning sidebands for the dephased spectrum is normalized by the intensity in the reference "full" spectrum

dx.doi.org/10.1021/ic500128y | Inorg. Chem. 2014, 53, 7146–7153

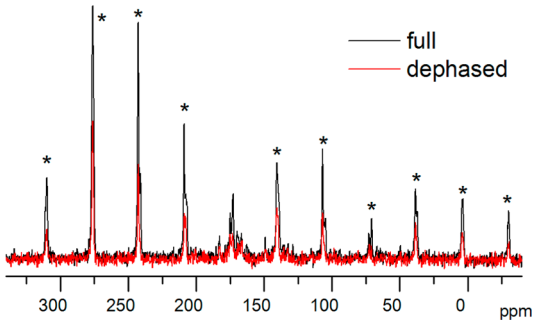

Figure 8. Full and dephased $^{13}C\{^{31}P\}$ REDOR spectra of [Ir(PyP)-(^{13}CO)Cl] acquired at 3.6 ms of dephasing time ($N \times T_r$) (* denotes spinning sidebands).

and is plotted as a data point that ranges between 1 and approximately −0.045 (*e.g.*, Figure 9). The functional form of

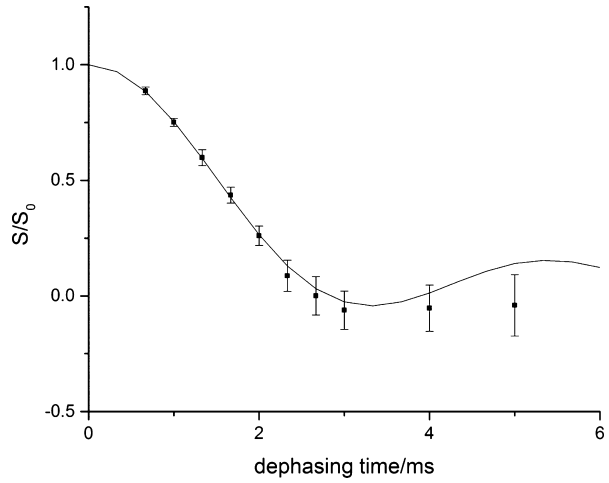

Figure 9. REDOR data and BS-REDOR reconstructed curve plotted as a function (S/S_0) for $^{13}C\{^{31}P\}$ REDOR of [Ir(PyP)(^{13}CO)Cl].

the REDOR curve for a given distance-dependent dipolar coupling is strictly prescribed. For the ^{13}C and ^{31}P spin pair, REDOR can measure distances accurately and precisely to about 8 Å. The precision of the distance measurement (r) is based partly on the r^{-3} dependence of the dipolar coupling.

Spectra that define complementary REDOR data points are shown in Figures 8 and 10 at similar dephasing times: In Figure 8, the enriched carbonyl ^{13}C nucleus is observed, selectively dephased by the 100% naturally abundant ^{31}P nucleus; in Figure 10, the 100% naturally abundant ^{31}P nucleus is observed, dephased by the enriched carbonyl ^{13}C nucleus.

Figures 9 and 11 show the series of data, derived from spectral pairs such as those in Figures 8 and 10, that are used to determine the ^{13}C−^{31}P internuclear distance. The increase in data error with dephasing time is due to the diminishing signal of the reference "full" spectrum under T_2 relaxation. The solid lines in Figures 9 and 11 are the curve reconstructions from the Boltzmann statistics REDOR analysis (BS-REDOR) approach developed by Gehman et al.[33] This approach employs Boltzmann statistics maximum entropy to determine an unbiased distribution of internuclear distances. For the ^{13}C-$\{^{31}P\}$ case, where all observed ^{13}C carbonyl nuclei are necessarily dephased by 100% naturally abundant ^{31}P, the widest conceivable distribution that is consistent with the data (per the theoretical basis of the analysis) is very narrow: 2.88 ± 0.02 Å, in reasonable agreement with the 2.83 Å distance obtained from single crystal diffraction studies. In the reciprocal experiment, ^{31}P is observed and dephased by possibly less than 100% enrichment at the ^{13}C carbonyl position. In this case, we must consider the effect of intermolecular contacts with neighboring carbonyl positions. In the crystal (the same sample preparation used for solid state NMR), the nearest intermolecular ^{13}C carbonyls are at 6.2, 6.5, and 7.6 Å. At the suffcient enrichment levels suggested by Figure 2b, these neighboring positions are unlikely to complicate the desired measurement where the closest ^{13}C nucleus is intramolecular, just as the analysis of the $^{13}C\{^{31}P\}$ data was uncomplicated. Where the intramolecular carbonyl carbon in not enriched, however, the corresponding ^{31}P nuclei will instead likely be dephased by one or more of the intermolecular carbonyl carbons. The BS-REDOR distribution supports these complications: while the peak intensity of 2.85 Å agrees with the measurements described above, the interquartile range of the

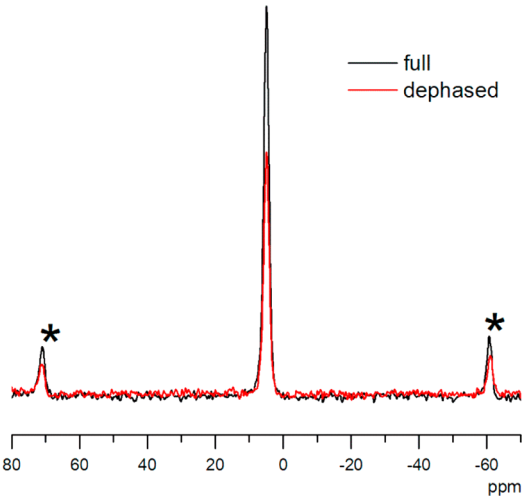

Figure 10. Full and dephased $^{31}P\{^{13}C\}$ REDOR spectra of [Ir(PyP)(^{13}CO)Cl] acquired at 3.5 ms dephasing. As for Figure 8, * denotes spinning sidebands at intervals of the 16 kHz magic angle spinning speed. This spin rate relative to the ^{31}P chemical shift anisotropy results in a majority of the density in the isotropic peak, with minor intensity in ±1 and spinning sidebands.

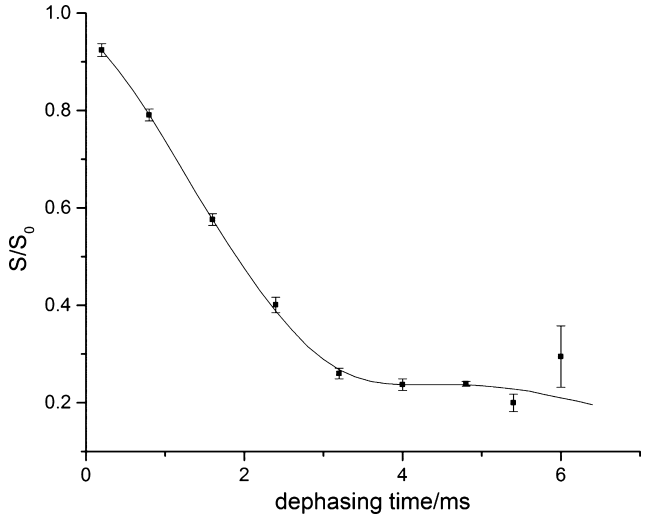

Figure 11. REDOR data and BS-REDOR reconstructed curve plotted as a function (S/S_0) for $^{31}P\{^{13}C\}$ REDOR of [Ir(PyP)(^{13}CO)Cl].

dx.doi.org/10.1021/ic500128y | *Inorg. Chem.* 2014, 53, 7146−7153

widest distribution consistent with the data ranges from 2.75 to 3.72 Å. The positive skew of this distribution reflects the aforementioned influence of intermolecular contacts with less than complete ^{13}C enrichment.

DISCUSSION

The solid-state techniques demonstrated here represent a heterogeneous selection of approaches for the characterization of metal complexes in the solid state. In our hands, the ultrafast MAS ^{1}H and CP MAS ^{13}C and ^{31}P NMR spectra provided information similar to that usually provided by their solution-state counterparts. Particularly, ^{1}H MAS spectra acquired at a MAS rate of 60 kHz provided very well-resolved resonances despite the low shift range of 10 ppm and could be recorded within seconds. High-resolution 2D correlation spectroscopy (a standard $^{1}H-^{13}C$ HETCOR) yielded dipolar-coupling contacts between proton and ^{13}C nuclei. In addition, we recorded the $^{1}H-^{31}P$ correlation with an additional spin diffusion block, which together yielded qualitative proximities between protons in [Ir(PyP)(^{13}CO)Cl] and these heteronuclei. The *anti* conformation of methylene protons in question in the ethylene bridge between the phosphine group and the pyrazole ring is directly confirmed by these experiments. The ^{1}H SQ–DQ correlation spectrum provided the dipolar coupling contacts between the protons located within 4 Å. These experiments rely on the extraordinary resolution obtained in the proton dimension at fast spinning speeds. Altogether, these experiments allowed us to assign the resonances we obtained and provided qualitative information about internuclear distances. In addition to the higher-sensitivity, qualitative proton-based proximities, we employed REDOR measurement for additional P–C distance information. These $^{31}P-^{13}C$ distance measurements were performed using both $^{13}C\{^{31}P\}$ and $^{31}P\{^{13}C\}$ REDOR. With this study being a proof-of-principle case, the $^{31}P-^{13}C$ internuclear distance and qualitative proton–proton contacts obtained could be compared to the distances observed in the crystal structure, which was reported for the unlabeled analogue [Ir(PyP)(CO)Cl] and turned out to be very similar. As a general limitation, mobility within the target compound will affect the dipolar coupling interaction in a way comparable to internuclear distance. The strategies shown are reasonable in cases where molecular structure is effectively rigid on the NMR time scale and may have to be adjusted when large differences in dynamics are expected.

Previous studies have mostly included relatively simple characterization techniques relying on isotropic heteronuclear shifts and shift anisotropy as well as specific extraction of parameters such as dipolar couplings or bonding patterns.[34−37] When primarily considering low-gamma nuclei and using comparably slow spinning speeds, useful information is also usually obtained only with considerable sample amounts.[38,39] In comparison to those studies, this work shows that a shift to high-gamma nuclei such as ^{1}H is useful and is becoming increasingly feasible with fast MAS. With the better filling factor of small rotors, isotopic enrichment for low-abundance isotope analysis of such small molecules is also now in reach. This opens up new routes particularly for characterization of supported catalysts.

Here, we present a combination of more traditional methods with experiments dedicated to fast MAS. Particularly, correlations between protons turn out to be a useful tool for obtaining structural parameters with reasonable sensitivity for low sample amounts. Correlations between ^{1}H chemical shifts and heteronuclei are also highly valuable and can be obtained with equally high resolution. Importantly, with the resolution obtained at 60 kHz MAS, simple single-quantum experiments are a valuable addition to the less sensitive double-quantum-based experiments. This is interesting particularly for future applications with a lower abundance of the species in focus. Similarly, the ^{1}H resolution obtained without high-power decoupling upon fast MAS is definitely comparable with windowed decoupling schemes and slow spinning. At the same time, temperature fluctuations upon B_1 irradiation are greatly reduced by low-power or omission of decoupling.

The solid-state NMR techniques demonstrated here can be applied to structure determination of compounds and materials which are insoluble and/or disordered in nature and therefore cannot be characterized with solution NMR and/or single-crystal X-ray diffraction. Particularly those materials raising difficulties due to their heterogeneity induced by a solid support will be a future target using similar approaches.

CONCLUSION

Fast magic angle spinning is shown here to be a versatile complement to traditional methods used for characterization of organometallic compounds. In combination with conventional methods, we show ^{1}H as the most abundant spin to be readily exploited for a number of correlation experimental details with high resolution and sensitivity. Generally, the methods toward resonance assignments and semiquantitative distances and proximities described here focus on those nuclei present in the ligand, which gives them broad applicability for transition metal complexes independent of the metal center. Whereas the traditional experiments require comparably long acquisition times even for the pure (but mostly unlabeled) material, the ^{1}H-based experiments are also comparably high in signal-to-noise and will be of major versatility for future studies of supportd transition metal complexes.

ASSOCIATED CONTENT

Supporting Information

NMR experiments, $^{1}H\{^{31}P\}$ spectrum of [Ir(PyP)(^{13}CO)Cl] recorded in CD_2Cl_2, $^{1}H-^{31}P$ correlation spectrum acquired at t_{mix} of 1000 μs, ^{1}H SQ-SQ correlation spectra acquired at t_{mix} of 2, 6, 80, and 300 μs. This material is available free of charge via the Internet at http://pubs.acs.org.

AUTHOR INFORMATION

Corresponding Author

*E-mail: b.messerle@unsw.edu.au.

Author Contributions

‖These authors contributed equally to the work. The manuscript was written through contributions of all authors. RL is now at the Max-Planck Institute for Biophysical Chemistry, Göttingen, Germany.

Notes

The authors declare no competing financial interest.

ACKNOWLEDGMENTS

A.A.T. thanks the Australian Government for the award of an IPRS (International Research Postgraduate Scholarship). R.L. is a DECRA fellow and acknowledges financial support from the Australian Research Council (ARC). J.D.G. acknowledges support as an ARC Future Fellow (FT0991558). This research

was supported under the Australian Research Council's Discovery Projects funding scheme (DP130101838), and financial support from UNSW is also gratefully acknowledged.

REFERENCES

(1) Bornils, B.; Herrmann, W. A. *Applied Homogeneous Catalysis with Organometallic Compounds*, Second ed.: Applications; Wiley-VCH: Hoboken, NJ, 2002; Vol. *1*.
(2) Fraile, J. M.; Garcia, J. I.; Herrerias, C. I.; Mayoral, J. A.; Pires, E. *Chem. Soc. Rev.* **2009**, *38*, 695.
(3) Rossini, A. J.; Zagdoun, A.; Lelli, M.; Lesage, A.; Coperet, C.; Emsley, L. *Acc. Chem. Res.* **2013**, *46*, 1942.
(4) Duckett, S. B.; Mewis, R. E. *Acc. Chem. Res.* **2012**, *45*, 1247.
(5) Laws, D. D.; Bitter, H. M. L.; Jerschow, A. *Angew. Chem., Int. Ed.* **2002**, *41*, 3096.
(6) Zhang, W. P.; Xu, S. T.; Han, X. W.; Bao, X. H. *Chem. Soc. Rev.* **2012**, *41*, 192.
(7) MacNamara, E.; Raftery, D. *J. Catal.* **1998**, *175*, 135.
(8) Abdulhussain, S.; Breitzke, H.; Ratajczyk, T.; Grunberg, A.; Srour, M.; Arnaut, D.; Weidler, H.; Kunz, U.; Kleebe, H. J.; Bommerich, U.; Bernarding, J.; Gutmann, T.; Buntkowsky, G. *Chem.—Eur. J.* **2014**, *20*, 1159.
(9) Wiench, J. W.; Michon, C.; Ellern, A.; Hazendonk, P.; Iuga, A.; Angelici, R. J.; Pruski, M. *J. Am. Chem. Soc.* **2009**, *131*, 11801.
(10) Bluemel, J. *Coord. Chem. Rev.* **2008**, *252*, 2410.
(11) Adamczyk, A.; Xu, Y.; Walaszek, B.; Roelofs, F.; Pery, T.; Pelzer, K.; Philippot, K.; Chaudret, B.; Limbach, H. H.; Breitzke, H.; Buntkowsky, G. *Top. Catal.* **2008**, *48*, 75.
(12) Joubert, J.; Delbecq, F.; Sautet, P.; Le Roux, E.; Taoufik, M.; Thieuleux, C.; Blanc, F.; Coperet, C.; Thivolle-Cazat, J.; Basset, J.-M. *J. Am. Chem. Soc.* **2006**, *128*, 9157.
(13) Mazoyer, E.; Trebosc, J.; Baudouin, A.; Boyron, O.; Pelletier, J.; Basset, J.-M.; Vitorino, M. J.; Nicholas, C. P.; Gauvin, R. M.; Taoufik, M.; Delevoye, L. *Angew. Chem., Int. Ed.* **2010**, *49*, 9854.
(14) Merle, N.; Trebosc, J.; Baudouin, A.; Del Rosal, I.; Maron, L.; Szeto, K.; Genelot, M.; Mortreux, A.; Taoufik, M.; Delevoye, L.; Gauvin, R. M. *J. Am. Chem. Soc.* **2012**, *134*, 9263.
(15) Samantaray, M. K.; Alauzun, J.; Gajan, D.; Kavitake, S.; Mehdi, A.; Veyre, L.; Lelli, M.; Lesage, A.; Emsley, L.; Coperet, C.; Thieuleux, C. *J. Am. Chem. Soc.* **2013**, *135*, 3193.
(16) Atiqullah, M.; Akhtar, M. N.; Faiz, M.; Moman, A.; Abu-Raqabah, A. H.; Khan, J. H.; Wazeer, M. I. *Surf. Interface Anal.* **2006**, *38*, 1319.
(17) Jezequel, M.; Dufaud, V.; Ruiz-Garcia, M. J.; Carrillo-Hermosilla, F.; Neugebauer, U.; Niccolai, G. P.; Lefebvre, F.; Bayard, F.; Corker, J.; Fiddy, S.; Evans, J.; Broyer, J. P.; Malinge, J.; Basset, J. M. *J. Am. Chem. Soc.* **2001**, *123*, 3520.
(18) Holmes, R. L.; Campbell, J. A.; Linser, R.; Hook, J. M.; Burford, R. P. *Polymer* **2011**, *52*, 4471.
(19) Brown, S. P. *Solid State Nucl. Mag.* **2012**, *41*, 1.
(20) Wickramasinghe, N. P.; Shaibat, M.; Ishii, Y. *J. Am. Chem. Soc.* **2005**, *127*, 5796.
(21) Carnevale, D.; Linde, A. J. P.; Bauer, G.; Bodenhausen, G. *Chem. Phys. Lett.* **2013**, *580*, 172.
(22) Swamy, S. K. K.; Karczmarska, A.; Makowska-Janusik, M.; Kassiba, A.; Dittmer, J. *ChemPhysChem* **2013**, *14*, 1864.
(23) Tregubov, A. A.; Vuong, K. Q.; Luais, E.; Gooding, J. J.; Messerle, B. A. *J. Am. Chem. Soc.* **2013**, *135*, 16429.
(24) Burling, S.; Field, L. D.; Messerle, B. A.; Khuong, Q. V.; Turner, P. *Dalton Trans.* **2003**, 4181.
(25) Takegoshi, K.; Nakamura, S.; Terao, T. *Chem. Phys. Lett.* **2001**, *344*, 631.
(26) Grommek, A.; Meier, B. H.; Ernst, M. *Chem. Phys. Lett.* **2006**, *427*, 404.
(27) Hing, A. W.; Vega, S.; Schaefer, J. *J. Magn. Reson.* **1992**, *96*, 205.
(28) Reif, B.; van Rossum, B. J.; Castellani, F.; Rehbein, K.; Diehl, A.; Oschkinat, H. *J. Am. Chem. Soc.* **2003**, *125*, 1488.
(29) Ishii, Y.; Tycko, R. *J. Magn. Reson.* **2000**, *142*, 199.
(30) Chevelkov, V.; van Rossum, B. J.; Castellani, F.; Rehbein, K.; Diehl, A.; Hohwy, M.; Steuernagel, S.; Engelke, F.; Oschkinat, H.; Reif, B. *J. Am. Chem. Soc.* **2003**, *125*, 7788.
(31) Feike, M.; Demco, D. E.; Graf, R.; Gottwald, J.; Hafner, S.; Spiess, H. W. *J. Magn. Reson., Ser. A* **1996**, *122*, 214.
(32) Gullion, T. *Concepts Magn. Reson.* **1998**, *10*, 277.
(33) Gehman, J. D.; Separovic, F.; Lu, K.; Mehta, A. K. *J. Phys. Chem. B* **2007**, *111*, 7802.
(34) Jakobsen, H. J.; Bildsoe, H.; Skibsted, J.; Brorson, M.; Gor'kov, P.; Gan, Z. *J. Magn. Reson.* **2010**, *202*, 173.
(35) Burgess, K. M. N.; Xu, Y.; Leclerc, M. C.; Bryce, D. L. *Inorg. Chem.* **2014**, *53*, 552.
(36) Feindel, K. W.; Ooms, K. J.; Wasylishen, R. E. *Phys. Chem. Chem. Phys.* **2007**, *9*, 1226.
(37) Ooms, K. J.; Bolte, S. E.; Baruah, B.; Choudhary, M. A.; Crans, D. C.; Polenova, T. *Dalton Trans.* **2009**, 3262.
(38) Eichele, K.; Nachtigal, C.; Jung, S.; Mayer, H. A.; Lindner, E.; Strobele, M. *Magn. Reson. Chem.* **2004**, *42*, 807.
(39) Harris, K. J.; Wasylishen, R. E. *Inorg. Chem.* **2009**, *48*, 2316.